Hindawi
Mathematical Problems in Engineering
Volume 2019, Article ID 8358176, 14 pages
https://doi.org/10.1155/2019/8358176

Research Article

A Finite Point Method for Solving the Time Fractional Richards' Equation

Xinqiang Qin and Xin Yang

Department of Applied Mathematics, Xi'an University of Technology, Xi'an, Shaanxi 710054, China

Correspondence should be addressed to Xinqiang Qin; xqqin2008@163.com

Received 9 January 2019; Revised 29 June 2019; Accepted 18 August 2019; Published 29 September 2019

Academic Editor: Chaudry M. Khalique

In this paper, we propose a numerical method for solving the time fractional Richards' equation. We first approximate the time fractional derivative of the mentioned equations by a scheme of order $O(\tau^{2-\alpha})$, $0 < a < 1$; then, we use the finite point method to approximate the spatial derivatives. Before the discrete spatial derivatives, we introduced the basic principles of the finite point method. We solve the one- and two-dimensional versions of these equations using the proposed method. Moreover, the stability properties of the discretized scheme related to time are theoretically analyzed. Numerical results showed the efficiency of the method presented in this paper.

1. Introduction

In recent years, the theory of fractional calculus and fractional differential equation has been widely used in many fields, such as mechanics, physics, biomathematics, engineering, automatic control, fractal, and so on. Richards' equation is a basic model for describing soil water movement. The multiscale heterogeneity of soil makes the nature of water diffusion process not consistent with the preconditions of applying Fick's law, which often reflects the abnormal diffusion phenomenon of soil water infiltration. In response to the above phenomenon, the fractional Richards' equation is proposed to describe the process of water movement in unsaturated soil [1, 2]. After years of research and practice, numerical simulation has become an effective technical means to simulate soil water flow and infiltration [3–5]. Pachepsky et al. [1] used the finite difference method to solve the time fractional Richard's equation. Chen et al. [6] used the finite difference method and Kansa method to discretize the time fractional derivatives and the space fractional derivatives, respectively, in solving the time fractional diffusion equation. Freitas et al. [7] proposed the modified fractional integral Richard's equation to predict the anomalous diffusion process of horizontal infiltration in unsaturated media.

Meshless methods have become very popular in physics and engineering for solving partial differential equations because they do not require mesh reorganization in solving large deformation and many discontinuous problems [8–10]. Meanwhile, a meshless method is not restricted by grid, and its basic idea is to arrange nodes according to certain rules in the solution domain, use shape function to represent unknown field variables in the local region, and finally form stiffness matrix equations to solve it [11]. Onate et al. [12, 13] proposed the finite point method, which first added the stability term to the equation, and then constructed the shape function by moving least squares and discretized the partial differential equation with the stability term by collocation method. Tiwari and Kuhnert [14] developed a finite pointset method, which uses Taylor expansion and weighted least squares to approximate spatial derivatives and uses collocation schemes to discretize equations. Shojaei et al. [15] used the meshless finite point method to solve elastodynamic problems through an explicit velocity. In the same year, Kamranian et al. [16] discussed

the two-dimensional initial boundary value problem associated with the sine-Gordon equation using the finite point method. Li and Qin [17] used the meshless finite point method to solve the time fractional convection-diffusion equations, and the numerical results show that this method has higher computational accuracy than the finite difference method. Previously, their work [17] used the finite point method to solve the time fractional linear convection-diffusion equations and obtained better results. Currently, the finite point method is used to solve the time fractional nonlinear soil water movement equation, which belongs to the convection-diffusion equation. The finite point method first applies a stability term to the governing equation and then uses the meshless collocation method to discretize the governing equation. The numerical results show that the calculation accuracy is better when the stability term is applied; that is, applying a stability term can reduce the calculation error and make the simulation result more accurate.

In this paper, we consider the time fractional Richards' equation as the following: for one-dimensional,

$$ {}_0^C D_t^\alpha \theta = \frac{\partial}{\partial z}\left(D(\theta)\frac{\partial \theta}{\partial z}\right) + \frac{\partial K(\theta)}{\partial z} + f, \quad z \in \Omega_1,\ t > 0, \tag{1} $$

subject to the following general initial and boundary conditions:

$$ \begin{aligned} &\theta(z,0) = \theta_0(z), \quad z \in \Omega_1, \\ &\theta(z,t) = \varphi(z,t), \quad z \in \partial\Omega_1,\ t > 0, \end{aligned} \tag{2} $$

and for two-dimensional,

$$ \begin{aligned} {}_0^C D_t^\alpha \theta = &\frac{\partial}{\partial x}\left(D(\theta)\frac{\partial \theta}{\partial x}\right) + \frac{\partial}{\partial z}\left(D(\theta)\frac{\partial \theta}{\partial z}\right) \\ &+ \frac{\partial K(\theta)}{\partial z} + f, \quad z \in \Omega_1,\ t > 0, \end{aligned} \tag{3} $$

subject to the following general initial and boundary conditions:

$$ \begin{aligned} &\theta(x,z,0) = \theta_0(x,z), \quad z \in \Omega_2, \\ &\theta(x,z,t) = \psi(x,z,t), \quad z \in \partial\Omega_2,\ t > 0, \end{aligned} \tag{4} $$

where $\Omega_1 = [0, L]$, $\Omega_2 = [0, L] \times [0, L]$, θ is soil water content, $D(\theta)$ is diffusivity, and $K(\theta)$ is water conductivity. Assume that the nonlinear term $D(\theta)$ satisfies $0 < m \le D(\theta) \le M$ for positive m, M. $K(\theta)$ satisfies $|K(\theta)| \le L|\theta|$ and $|K'(\theta)| \le L$, where L is the different positive constant.

In equations (1) and (3), ${}_0^C D_t^\alpha \theta$ is the Caputo fractional derivative of order α ($0<\alpha<1$), which is defined as

$$ {}_a^C D_t^\alpha \theta(t) = \frac{1}{\Gamma(1-\alpha)} \int_\alpha^t \frac{\theta'(s)}{(t-s)^\alpha} ds. \tag{5} $$

Equations (1) and (3) belong to the part of soil water and salt transport model. Aiming at the convection and dispersion phenomenon in the soil water and salt transport model, the finite element method (FEM) and finite difference method (FDM) are easy to produce numerical oscillation when convection is dominant. Numerical methods such as characteristic finite element and characteristic finite difference can eliminate numerical oscillation to a certain extent, but these numerical methods need to rely on the grid in the calculation process, which increases the calculation amount. The meshless method defines the shape function at the nodes in the local domain, which overcomes the dependence on the grid in numerical calculation. Meanwhile, by adding nodes in the computational domain, the computational accuracy in the local region can be improved. The finite point method uses the moving least squares (MLS) method to construct the shape function and the collocation method to discretize the governing equation, which belongs to the meshless method. For equations (1) and (3), the time fractional Caputo derivatives were approximated by $L1$ interpolation, and the space derivatives were discredited by finite point method.

The paper is organized as follows: The finite point method is introduced in Section 2. The scheme of discrete time fractional soil water movement equations is deduced in Section 3. In Section 4, the stability of the time discretization of the one-dimensional and two-dimensional time fractional soil water movement equations is analyzed. In Section 5, some numerical examples are provided to show the accuracy of the proposed method. Finally, a conclusion is drawn in Section 6.

2. Finite Point Method

The finite point method (FPM) uses the moving least squares (MLS) method to construct the shape function and the collocation method to discretize the governing equations. In order to reduce the error and avoid the numerical oscillation, the stability term is added to the discrete equation [12, 13].

2.1. Moving Least Squares (MLS) Approximation. In (0, L), the unknown function $u(x)$ can be approximated in the neighborhood Ω_x of the point x:

$$ \begin{aligned} u(x) \approx u^h(x) = \sum_{i=1}^N \varphi_i(x) u_i = \Phi(x) U, \quad x \in \overline{\Omega}, \\ U = (u_1, u_2, \ldots, u_N)^T, \end{aligned} \tag{6} $$

where $\Phi(x)$ is the vector of MLS shape functions corresponding to N nodes in the support domain of the point x and can be expressed by

$$ \Phi(x) = p^T(x) A^{-1}(x) B(x), \tag{7} $$

where $p^T(x) = (p_1(x), p_2(x), \ldots, p_m(x))$ is a complete monomials basis of order m. $A(x)$ and $B(x)$ are defined by

$$ \begin{aligned} A(x) &= \sum_{i=1}^N W_i(x) p(x_i) p^T(x_i), \\ B(x) &= [W_1(x)p(x_1) W_1(x)p(x_1), \ldots, W_N(x)p(x_N)]. \end{aligned} \tag{8} $$

Let $\gamma = A^{-1}p$, then shape function is $\Phi^T = \gamma^T B$. The partial derivatives of the shape functions are, respectively,

$$\begin{aligned}\Phi_{,i}^{T} &= \gamma_{,i}^{T}B + \gamma^{T}B_{,i},\\ \Phi_{,ij}^{T} &= \gamma_{,ij}^{T}B + \gamma_{,i}^{T}B_{,j} + \gamma^{T}B_{,ij},\\ \Phi_{,ijk}^{T} &= \gamma_{,ijk}^{T}B + \gamma_{,ij}^{T}B_{,k} + \gamma_{,ik}^{T}B_{,j} + \gamma_{,jk}^{T}B_{,i} + \gamma_{,i}^{T}B_{,jk} + \gamma_{,j}^{T}B_{,ik}\\ &\quad + \gamma_{,k}^{T}B_{,ij} + \gamma^{T}B_{,ijk}.\end{aligned} \tag{9}$$

From the expression of the shape functions, we can see that the smoothness of the shape function is determined by the weight function, i.e., if $w(x - x_i) \in C^k(\Omega)$, $i = 1, 2, \ldots, n$, then $\phi_i(\mathrm{x}) \in C^k(\Omega)$. In the present work, Gaussian weight function with compact supports are considered, which is defined as

$$w(\mathbf{x}) = \begin{cases} \dfrac{e^{-r^2\beta^2} - e^{-\beta^2}}{1 - e^{-\beta^2}}, & r \le 1,\\ 0, & r > 1,\end{cases} \tag{10}$$

where β is the shape parameter of the Gaussian function and r is the relative distance:

$$r = \frac{d_i}{d_{mi}} = \frac{|x - x_i|}{d_{mi}}, \tag{11}$$

where d_i is the distance between the calculation point x and the node x_i, and d_{mi} is the support domain size of weight function. The support domain size d_{mi} of node x_i is usually determined by $d_{mi} = \text{scale} \cdot d_c$, where scale is the impact factor and d_c is used to control the size of the support domain. $d_i = \sqrt{(x - x_i)^2 + (y - y_i)^2}$ in the two-dimensional case.

2.2. Adding Stability Term. The one-dimensional time fractional soil water movement equation is shown in equation (1). Let

$$r = \frac{\partial K(\theta)}{\partial \theta} \cdot \frac{\partial \theta}{\partial z} + D(\theta)\frac{\partial^2 \theta}{\partial z^2} + \frac{\partial D(\theta)}{\partial \theta}\left(\frac{\partial \theta}{\partial z}\right)^2 + f. \tag{12}$$

Using Taylor's expansion and flow balance principles, the stability term is

$$R = \frac{h}{2} \cdot \frac{\partial r}{\partial z}, \tag{13}$$

where h is the characteristic length ([12, 13]).

After adding the stability term, equation (1) can be converted into the following form:

$${}_0^C D_t^{\alpha}\theta - r + \frac{h}{2} \cdot \frac{\partial r}{\partial z} = 0. \tag{14}$$

Similarly, equation (3) can be converted into the following form:

$${}_0^C D_t^{\alpha}\theta - r + \frac{h}{2|u|} \cdot u \cdot \nabla r = 0, \tag{15}$$

where

$$\begin{aligned} r &= \frac{\partial K(\theta)}{\partial \theta} \cdot \frac{\partial \theta}{\partial z} + \frac{\partial K(\theta)}{\partial \theta} \cdot \frac{\partial \theta}{\partial x} + D(\theta)\frac{\partial^2 \theta}{\partial x^2} + \frac{\partial D(\theta)}{\partial \theta}\left(\frac{\partial \theta}{\partial x}\right)^2\\ &\quad + D(\theta)\frac{\partial^2 \theta}{\partial z^2} + \frac{\partial D(\theta)}{\partial \theta}\left(\frac{\partial \theta}{\partial z}\right)^2 + f - \frac{\partial K(\theta)}{\partial \theta} \cdot \frac{\partial \theta}{\partial x},\end{aligned} \tag{16}$$

gradient ∇r

$$\nabla r = \left[\frac{\partial r}{\partial x}, \frac{\partial r}{\partial z}\right]^T, \tag{17}$$

the coefficient of convection term $u = [-(\partial K(\theta)/\partial\theta), -(\partial K(\theta)/\partial\theta)]$, and h is the characteristic length.

2.3. Collocation Method. Assume that the equation is as follows:

$$L[u(x)] = f(x), \quad x \in \Omega. \tag{18}$$

The Dirichlet boundary condition is

$$u - u_p = 0, \quad x \in \Gamma_u. \tag{19}$$

The Neumann boundary condition is

$$B(u) = g(x), \quad x \in \Gamma_t, \tag{20}$$

where L and B are the differential operators, u is the unknown function, u_p is the prescribed value of u in Γ_u, the boundary $\partial\Omega = \Gamma = \Gamma_t \cup \Gamma_u$, and $\Gamma_t \cap \Gamma_u = 0$ in Ω.

Assume the approximate expression of u is $\hat{u}$; then, the approximate function will inevitably produce residuals in the domain and on the boundary, respectively. By using the weighted residual method, equations (18)–(20) are replaced by the following formula:

$$\begin{aligned}&\int_{\Omega} W_1[L(\hat{u}) - f(x)]d\Omega + \int_{\Gamma_t} W_2[B(\hat{u}) - g(x)]d\Gamma\\ &\quad + \int_{\Gamma_u} W_3\left[\hat{u} - u_p\right]d\Gamma,\end{aligned} \tag{21}$$

the weight functions W_1, W_2, and W_3 have different definitions. Let $W_1 = W_2 = W_3 = \delta_i$, where δ_i is the Dirac δ function, from which the point equation can be obtained as

$$L[\hat{u}(x_i)] - f(x_i) = 0, \quad x_i \in \Omega,\ i = 1, \ldots, n_d, \tag{22}$$

$$\begin{aligned}&u(x_i) - u_p = 0,\\ &\qquad x_i \in \Gamma_u,\ i = n_d + n_t + 1, \ldots, n_d + n_t + n_u,\end{aligned} \tag{23}$$

$$B(\hat{u}(x_i)) - g(x_i) = 0, \quad x_i \in \Gamma_t,\ i = n_d + 1, \ldots, n_d + n_t, \tag{24}$$

where n_u is the number of nodes on the Dirichlet boundary, n_t is the number of nodes on the Neumann boundary, n_d is the number of nodes which satisfy $n_d = N\text{-}n_t\text{-}n_u$ in Ω. The

system of equations (22)–(24) leads to a system of algebraic equations of the form

$$Ku_p = F. \tag{25}$$

If the differential operators L and B are nonlinear, it is a nonlinear system of equations, and the approximate value of nodes should be solved by the iterative method [18–21]. Monotone iterative ADI (alternating direction implicit) was used for solving coupled systems of nonlinear parabolic equations, and Boglaev [19] stopped the algorithm and the number of iterations by verifying the convergence order. The inexact Hermitian/Skew-Hermitian Splitting (IHSS) was presented for solving system of nonlinear equations [20]. The stopped criterion for the outer iterations in INHSS algorithm were $\|F(u^k)\|/\|F(u^0)\| \le \delta$, where δ is a prescribed accuracy. A novel biparametric six-order iterative scheme for solving nonlinear systems was presented by Bahl et al. [21]. The number of iterations needed to converge to the solution such that the stopping criterion $\|\mathbf{x}^{(k+1)} - \mathbf{x}^{(k)}\| + \|\mathbf{F}(\mathbf{x})^{(k)}\| < 10^{\delta}$ was satisfied [21].

3. Algorithm Construction of Time Fractional Soil Water Movement Equation

3.1. In the One-Dimensional Case

3.1.1. Time Discretization. Let $t_m = m\Delta t$, $m = 1, 2, \ldots, n$, where $\Delta t = T/n$ is time step. The time fractional derivative at $t = t_m$ can be approximated by the following scheme:

$$\begin{aligned} {}_0^C D_t^{\alpha}\theta(t)|_{t=t_m} &= \frac{1}{\Gamma(1-\alpha)}\sum_{k=1}^{m}\int_{t_{k-1}}^{t_k}\frac{\theta(t_k)-\theta(t_{k-1})}{\Delta t} \\ &\quad\cdot\frac{1}{(t_n-s)^{\alpha}}ds + \widetilde{R}_m \\ &= \frac{\tau^{-\alpha}}{\Gamma(2-\alpha)}\left[a_0^{(\alpha)}\theta(t_m) - \sum_{k=1}^{m-1}\left(a_{m-k-1}^{(\alpha)} - a_{m-k}^{(\alpha)}\right)\theta(t_k)\right. \\ &\quad \left. - a_{m-1}^{(\alpha)}\theta(t_0)\right] + \widetilde{R}_m, \end{aligned} \tag{26}$$

where

$$\begin{aligned} a_{m-k-1}^{(\alpha)} &= (m-k)^{1-\alpha} - (m-k-1)^{1-\alpha}, \\ a_{m-k}^{(\alpha)} &= (m-k+1)^{1-\alpha} - (m-k)^{1-\alpha}, \end{aligned} \tag{27}$$

and the truncation error is

$$\left|\widetilde{R}_m\right| \le C(\Delta t)^{2-\alpha}. \tag{28}$$

So, the $L1$ approximation of Caputo derivative is

$${}_0^C D_t^{\alpha}\theta(t)|_{t=t_m} \approx \frac{\tau^{-\alpha}}{\Gamma(2-\alpha)}\left[a_0^{(\alpha)}\theta(t_m) - \sum_{k=1}^{m-1}\left(a_{m-k-1}^{(\alpha)} - a_{m-k}^{(\alpha)}\right)\theta(t_k) - a_{m-1}^{(\alpha)}\theta(t_0)\right]. \tag{29}$$

Let $\theta^m = \theta^m(x)$ be the numerical approximation to $\theta(x, t_m)$ and $f^m = f(x, t_m)$; then, equation (1) can be discretized as the following scheme:

$$\begin{aligned} &\frac{\tau^{-\alpha}}{\Gamma(2-\alpha)}\left[a_0^{(\alpha)}\theta^m - \sum_{k=1}^{m-1}\left(a_{m-k-1}^{(\alpha)} - a_{m-k}^{(\alpha)}\right)\theta^k - a_{m-1}^{(\alpha)}\theta^0\right] \\ &\quad = \frac{\partial}{\partial z}\left(D(\theta^m)\frac{\partial\theta^m}{\partial z}\right) + \frac{\partial K(\theta^m)}{\partial z} + f^m. \end{aligned} \tag{30}$$

3.1.2. Spatial Discretization. Equation (1) can be transformed into

$${}_0^C D_t^{\alpha}\theta - \frac{\partial K(\theta)}{\partial\theta}\cdot\frac{\partial\theta}{\partial z} - D(\theta)\frac{\partial^2\theta}{\partial z^2} - \frac{\partial D(\theta)}{\partial\theta}\left(\frac{\partial\theta}{\partial z}\right)^2 - f = 0. \tag{31}$$

After adding the stability term to equation (31), we can obtain

$$\begin{aligned} &{}_0^C D_t^{\alpha}\theta - \left(\frac{\partial K(\theta)}{\partial\theta}\cdot\frac{\partial\theta}{\partial z} + D(\theta)\frac{\partial^2\theta}{\partial z^2} + \frac{\partial D(\theta)}{\partial\theta}\left(\frac{\partial\theta}{\partial z}\right)^2 + f\right) \\ &\quad - \frac{h}{2}\left[-\left(\frac{\partial^2 K(\theta)}{\partial^2\theta}\left(\frac{\partial\theta}{\partial z}\right)^2 + \frac{\partial K(\theta)}{\partial\theta}\cdot\frac{\partial^2\theta}{\partial z^2} + 3\frac{\partial D(\theta)}{\partial\theta}\right.\right. \\ &\quad \left.\left.\cdot\frac{\partial\theta}{\partial z}\cdot\frac{\partial^2\theta}{\partial z^2} + D(\theta)\frac{\partial^3\theta}{\partial z^3} + \frac{\partial^2 D(\theta)}{\partial\theta^2}\left(\frac{\partial\theta}{\partial z}\right)^3 + \frac{\partial f}{\partial z}\right)\right] = 0. \end{aligned} \tag{32}$$

The N nodes $z = z_i$ $(i = 1, 2, \ldots, N)$ in the domain (a, b) are used for the distribution, and the approximate function at the node z_p is

$$\theta(z_p) \cong \widehat{\theta}(z_p) = \sum_{i=1}^{N}\varphi_{pi}(z_p)\theta(z_i), \tag{33}$$

where φ_{pi} represents the shape function formed by z_p as the support domain center and the point z_i, and N is the number of nodes in the local support domain with z_p as the support domain center.

From equation (33), the first derivative, the second derivative, and the third derivative of the approximation function at the node z_p can be expressed as

$$\begin{cases} \left.\dfrac{\partial\theta(z)}{\partial z}\right|_{z=z_p} = \displaystyle\sum_{i=1}^{N}\left.\frac{\partial\varphi_{pi}(z)}{\partial z}\theta(z_i)\right|_{z=z_p}, \\ \left.\dfrac{\partial^2\theta(z)}{\partial z^2}\right|_{z=z_p} = \displaystyle\sum_{i=1}^{N}\left.\frac{\partial^2\varphi_{pi}(z)}{\partial z^2}\theta(z_i)\right|_{z=z_p}, \\ \left.\dfrac{\partial^3\theta(z)}{\partial z^3}\right|_{z=z_p} = \displaystyle\sum_{i=1}^{N}\left.\frac{\partial^3\varphi_{pi}(z)}{\partial z^3}\theta(z_i)\right|_{z=z_p}. \end{cases} \tag{34}$$

Substititing equations (33) and (34) in equation (32), we can obtain the spatial discrete equation.

Let θ_p^m be the numerical approximation to $\theta(z_p, t_m)$, from equations (29) and (33)–(35), the fully discrete scheme of equation (1) at $\theta(z_p, t_m)$ is

$$\begin{aligned}
&\frac{\tau^{-\alpha}}{\Gamma(2-\alpha)}\left[a_0^{(\alpha)}\theta_p^m - \sum_{k=1}^{m-1}\left(a_{m-k-1}^{(\alpha)} - a_{m-k}^{(\alpha)}\right)\theta_p^k - a_{m-1}^{(\alpha)}\theta_p^0\right] \\
&= \sum_{i=1}^{N}\alpha_{pi}\cdot\theta_i^m + \left[\left(\frac{\partial D(\theta^m)}{\partial\theta} - \frac{h}{2}\frac{\partial^2 K(\theta^m)}{\partial\theta^2}\right)\left(\sum_{i=1}^{N}\frac{\partial\phi_{pi}}{\partial z}\cdot\theta_i^m\right)^2\right. \\
&- \frac{3h}{2}\frac{\partial D(\theta^m)}{\partial\theta}\left(\sum_{i=1}^{N}\frac{\partial\phi_{pi}}{\partial z}\cdot\theta_i^m\right) \\
&\cdot\left(\sum_{i=1}^{N}\frac{\partial^2\phi_{pi}}{\partial z^2}\cdot\theta_i^m\right) - \frac{h}{2}\frac{\partial^2 D(\theta^m)}{\partial\theta^2}\left(\sum_{i=1}^{N}\frac{\partial\phi_{pi}}{\partial z}\cdot\theta_i^m\right)^3 \\
&\left. -\frac{h}{2}\frac{\partial f^m}{\partial z}\bigg|_{z=z_p} + f_p^m\right],
\end{aligned} \tag{35}$$

where

$$\begin{aligned}
\alpha_{pi}^m = &\left(\frac{\partial K(\theta^m)}{\partial\theta}\frac{\partial\varphi_{pi}}{\partial z}\bigg|_{z=z_p} + \left(D\left(\theta_p^m\right) - \frac{h}{2}\frac{\partial K(\theta^m)}{\partial\theta}\right)\frac{\partial^2\varphi_{pi}}{\partial z^2}\bigg|_{z=z_p}\right. \\
&\left. -\frac{h}{2}D\left(\theta_p^m\right)\frac{\partial^3\varphi_{pi}}{\partial z^3}\bigg|_{z=z_p}\right).
\end{aligned} \tag{36}$$

Let

$$\theta^m = \left(\theta_1^m, \theta_2^m, \ldots, \theta_p^m, \ldots, \theta_N^m\right)^T, \quad m = 1, 2, 3, \ldots. \tag{37}$$

Equation (35) is as follows:

$$\begin{aligned}
P^m\theta^m = &\frac{\tau^{-\alpha}}{\Gamma(2-\alpha)}\sum_{k=1}^{m-1}\left(a_{m-k-1}^{(\alpha)} - a_{m-k}^{(\alpha)}\right)\theta^k \\
&+ \frac{\tau^{-\alpha}}{\Gamma(2-\alpha)}a_{m-1}^{(\alpha)}\theta^0 + F^m,
\end{aligned} \tag{38}$$

where

$$\begin{aligned}
P^m = &\left(\frac{\tau^{-\alpha}}{\Gamma(2-\alpha)}a_0^{(\alpha)}\cdot E - A - \left(\frac{\partial D(\theta^m)}{\partial\theta} - \frac{h}{2}\frac{\partial^2 K(\theta^m)}{\partial\theta^2}\right)\right. \\
&\cdot\left(\sum_{i=1}^{N}\frac{\partial\varphi_{pi}}{\partial z}\cdot\theta_i^m\right)\cdot B \\
&+ \frac{3h}{2}\cdot\frac{\partial D(\theta^m)}{\partial\theta}\left(\sum_{i=1}^{N}\frac{\partial^2\varphi_{pi}}{\partial z^2}\cdot\theta_i^m\right) \\
&\left.\cdot C + \frac{h}{2}\cdot\frac{\partial^2 D(\theta^m)}{\partial\theta^2}\left(\sum_{i=1}^{N}\frac{\partial\varphi_{pi}}{\partial z}\cdot\theta_i^m\right)^2\cdot B\right),
\end{aligned}$$

$$A = \begin{bmatrix} \alpha_{11} & \alpha_{12} & \cdots & \alpha_{1N} \\ \alpha_{21} & \alpha_{22} & \cdots & \alpha_{2N} \\ \vdots & \vdots & \vdots & \vdots \\ \alpha_{p1} & \alpha_{p2} & \cdots & \alpha_{pN} \\ \vdots & \vdots & \vdots & \vdots \\ \alpha_{N1} & \alpha_{N2} & \cdots & \alpha_{NN} \end{bmatrix},$$

$$B = \begin{bmatrix} \frac{\partial\varphi_{11}}{\partial z} & \frac{\partial\varphi_{12}}{\partial z} & \cdots & \frac{\partial\varphi_{1N}}{\partial z} \\ \frac{\partial\varphi_{21}}{\partial z} & \frac{\partial\varphi_{22}}{\partial z} & \cdots & \frac{\partial\varphi_{2N}}{\partial z} \\ \vdots & \vdots & \vdots & \vdots \\ \frac{\partial\varphi_{p1}}{\partial z} & \frac{\partial\varphi_{p2}}{\partial z} & \cdots & \frac{\partial\varphi_{pN}}{\partial z} \\ \vdots & \vdots & \vdots & \vdots \\ \frac{\partial\varphi_{N1}}{\partial z} & \frac{\partial\varphi_{N2}}{\partial z} & \cdots & \frac{\partial\varphi_{NN}}{\partial z} \end{bmatrix},$$

$$C = \begin{bmatrix} \frac{\partial^2\varphi_{11}}{\partial z^2} & \frac{\partial^2\varphi_{12}}{\partial z^2} & \cdots & \frac{\partial^2\varphi_{1N}}{\partial z^2} \\ \frac{\partial^2\varphi_{21}}{\partial z^2} & \frac{\partial^2\varphi_{22}}{\partial z^2} & \cdots & \frac{\partial^2\varphi_{2N}}{\partial z^2} \\ \vdots & \vdots & \vdots & \vdots \\ \frac{\partial^2\varphi_{p1}}{\partial z^2} & \frac{\partial^2\varphi_{p2}}{\partial z^2} & \cdots & \frac{\partial^2\varphi_{pN}}{\partial z^2} \\ \vdots & \vdots & \vdots & \vdots \\ \frac{\partial^2\varphi_{N1}}{\partial z^2} & \frac{\partial^2\varphi_{N2}}{\partial z^2} & \cdots & \frac{\partial^2\varphi_{NN}}{\partial z^2} \end{bmatrix},$$

$$F = \begin{bmatrix} -\frac{h}{2}\cdot\frac{\partial f^m}{\partial z}\Big|_{z=z_1} + f_1^m \\ -\frac{h}{2}\cdot\frac{\partial f^m}{\partial z}\Big|_{z=z_2} + f_2^m \\ \vdots \\ -\frac{h}{2}\cdot\frac{\partial f^m}{\partial z}\Big|_{z=z_p} + f_p^m \\ \vdots \\ -\frac{h}{2}\cdot\frac{\partial f^m}{\partial z}\Big|_{z=z_N} + f_N^m \end{bmatrix}. \tag{39}$$

3.2. In the Two-Dimensional Case

3.2.1. Time Discretization. Let $t_m = m\Delta t$, $m = 1, 2, \ldots, n$, where $\Delta t = T/n$ is the time step, the approximation of the time fractional derivative at $t = t_m$ is shown in equation (29). Let $\theta^m = \theta^m(x, z)$ be the numerical approximation to $\theta(x, z, t_m)$ and $f^m = f(x, z, t_m)$; then, equation (3) can be discretized as the following scheme:

$$\frac{\tau^{-\alpha}}{\Gamma(2-\alpha)}\left[a_0^{(\alpha)}\theta^m-\sum_{k=1}^{m-1}\left(a_{m-k-1}^{(\alpha)}-a_{m-k}^{(\alpha)}\right)\theta^k-a_{m-1}^{(\alpha)}\theta^0\right]$$
$$=\frac{\partial}{\partial x}\left(D\left(\theta^m\right)\frac{\partial\theta^m}{\partial x}\right)+\frac{\partial}{\partial z}\left(D\left(\theta^m\right)\frac{\partial\theta^m}{\partial z}\right)+\frac{\partial K\left(\theta^m\right)}{\partial z}+f^m. \tag{40}$$

3.2.2. Spatial Discretization. The governing equation (3) can be rewritten as

$$ {}_0^C D_t^\alpha\theta-\frac{\partial K(\theta)}{\partial\theta}\cdot\frac{\partial\theta}{\partial z}-D(\theta)\frac{\partial^2\theta}{\partial x^2}-\frac{\partial D(\theta)}{\partial\theta}\left(\frac{\partial\theta}{\partial x}\right)^2-D(\theta)\frac{\partial^2\theta}{\partial z^2}-\frac{\partial D(\theta)}{\partial\theta}\left(\frac{\partial\theta}{\partial z}\right)^2-f=0. \tag{41}$$

From Section 2.2, it can be seen that the two-dimensional fractional soil-water movement equation after adding the stable term is

$$ {}_0^C D_t^\alpha\theta-r+\frac{h}{2|u|}\cdot u\cdot\nabla r=0, \tag{42}$$

where $r,\nabla r,u$ are shown in Section 2.2. Then, equation (3) can be converted into

$$\begin{aligned}
&{}_0^C D_t^\alpha\theta-\frac{\partial K(\theta)}{\partial\theta}\cdot\frac{\partial\theta}{\partial z}-D(\theta)\frac{\partial^2\theta}{\partial x^2}-\frac{\partial D(\theta)}{\partial\theta}\left(\frac{\partial\theta}{\partial x}\right)^2-D(\theta)\frac{\partial^2\theta}{\partial z^2}-\frac{\partial D(\theta)}{\partial\theta}\left(\frac{\partial\theta}{\partial z}\right)^2-f\\
&+\frac{h}{2|u|}\left[-\frac{\partial K(\theta)}{\partial\theta}\left(\frac{\partial^2K(\theta)}{\partial\theta^2}\cdot\frac{\partial\theta}{\partial x}\cdot\frac{\partial\theta}{\partial z}+\frac{\partial K(\theta)}{\partial\theta}\cdot\frac{\partial^2\theta}{\partial z\,\partial x}+3\frac{\partial D(\theta)}{\partial\theta}\cdot\frac{\partial\theta}{\partial x}\cdot\frac{\partial^2\theta}{\partial x^2}+D(\theta)\frac{\partial^3\theta}{\partial x^3}\right.\right.\\
&+\frac{\partial^2D(\theta)}{\partial\theta^2}\left(\frac{\partial\theta}{\partial x}\right)^3+\frac{\partial D(\theta)}{\partial\theta}\cdot\frac{\partial\theta}{\partial x}\cdot\frac{\partial^2\theta}{\partial z^2}+\frac{\partial^2D(\theta)}{\partial\theta^2}\cdot\frac{\partial\theta}{\partial x}\cdot\left(\frac{\partial\theta}{\partial z}\right)^2+\frac{\partial f}{\partial x}+D(\theta)\frac{\partial^3\theta}{\partial z^2\partial x}\\
&+2\frac{\partial D(\theta)}{\partial\theta}\cdot\frac{\partial\theta}{\partial z}\cdot\frac{\partial^2\theta}{\partial z\,\partial x}\Bigg)-\frac{\partial K(\theta)}{\partial\theta}\left(\frac{\partial^2K(\theta)}{\partial\theta^2}\left(\frac{\partial\theta}{\partial z}\right)^2+\frac{\partial K(\theta)}{\partial\theta}\cdot\frac{\partial^2\theta}{\partial z^2}+\frac{\partial D(\theta)}{\partial\theta}\cdot\frac{\partial\theta}{\partial z}\cdot\frac{\partial^2\theta}{\partial x^2}\right.\\
&+D(\theta)\frac{\partial^3\theta}{\partial x^2\partial z}+3\frac{\partial D(\theta)}{\partial\theta}\cdot\frac{\partial\theta}{\partial z}\cdot\frac{\partial^2\theta}{\partial z^2}+D(\theta)\frac{\partial^3\theta}{\partial z^3}+\frac{\partial^2D(\theta)}{\partial\theta^2}\cdot\frac{\partial\theta}{\partial z}\cdot\left(\frac{\partial\theta}{\partial x}\right)^2+2\frac{\partial D(\theta)}{\partial\theta}\\
&\left.\left.\cdot\frac{\partial\theta}{\partial x}\cdot\frac{\partial^2\theta}{\partial x\,\partial z}+\frac{\partial^2D(\theta)}{\partial\theta^2}\cdot\left(\frac{\partial\theta}{\partial z}\right)^3+\frac{\partial f}{\partial z}\right)\right]=0.
\end{aligned} \tag{43}$$

The approximate function at $\theta(x_p,z_q)$ is

$$\theta\left(x_p,z_q\right)=\sum\varphi_{pq,ij}\left(x_p,z_q\right)\cdot\theta\left(x_i,z_j\right), \tag{44}$$

where $\varphi_{pq,ij}$ represents the shape function formed by $\theta(x_p,z_q)$ as the center of the support domain and $\theta(x_i,z_j)$.

The approximate expressions of the unknown function, the first derivative, the second derivative, and the third derivative of the unknown function at $\theta(x_p,z_q)$ can be obtained by constructing the shape function. So, the full discrete scheme of equation (3) at $\theta(x_p,z_q,t_m)$ is as follows:

$$
\begin{aligned}
&\frac{\tau^{-\alpha}}{\Gamma(2-\alpha)}\left[a_0^{(\alpha)}\theta_{pq}^m-\sum_{k=1}^{m-1}\left(a_{m-k-1}^{(\alpha)}-a_{m-k-1}^{(\alpha)}\right)-a_{m-1}^{(\alpha)}\theta_{pq}^0\right]=\sum_{ij}\left[\frac{\partial K(\theta^m)}{\partial\theta}\frac{\partial\varphi_{pq,ij}}{\partial z}+D\left(\theta_{pq}^m\right)\right.\\
&\cdot\frac{\partial^2\varphi_{pq,ij}}{\partial x^2}+D\left(\theta_{pq}^m\right)\frac{\partial^2\varphi_{pq,ij}}{\partial z^2}+\frac{h}{2|u|}\frac{\partial K(\theta^m)}{\partial\theta}\cdot\frac{\partial^2K(\theta^m)}{\partial\theta^2}\cdot\frac{\partial^2\varphi_{pq,ij}}{\partial x\,\partial z}+\frac{h}{2|u|}\left(\frac{\partial K(\theta^m)}{\partial\theta}\right)^2\frac{\partial^2\varphi_{pq,ij}}{\partial z\,\partial x}\\
&+\frac{h}{2|u|}\frac{\partial K(\theta^m)}{\partial\theta}\cdot D(\theta^m)\cdot\frac{\partial^3\varphi_{pq,ij}}{\partial x^3}+\frac{h}{2|u|}\frac{\partial K(\theta^m)}{\partial\theta}\cdot D(\theta^m)\cdot\frac{\partial^3\varphi_{pq,ij}}{\partial z^2\partial x}+\frac{h}{2|u|}\left(\frac{\partial K(\theta^m)}{\partial\theta}\right)^2\frac{\partial^2\varphi_{pq,ij}}{\partial z^2}\\
&\left.+\frac{h}{2|u|}\frac{\partial K(\theta^m)}{\partial\theta}\cdot D(\theta^m)\cdot\frac{\partial^3\varphi_{pq,ij}}{\partial x^2\partial z}+\frac{h}{2|u|}\frac{\partial K(\theta^m)}{\partial\theta}\cdot D(\theta^m)\cdot\frac{\partial^3\varphi_{pq,ij}}{\partial z^3}\right]\Bigg|_{\theta=\theta\left(x_p,z_q\right)}\cdot\theta_{ij}^m+\left\{\frac{\partial D(\theta^m)}{\partial\theta}\right.\\
&\cdot\left(\sum_{ij}\frac{\partial\varphi_{pq,ij}}{\partial x}\theta_{ij}^m\right)^2+\frac{\partial D(\theta^m)}{\partial\theta}\left(\sum_{ij}\frac{\partial\varphi_{pq,ij}}{\partial z}\theta_{ij}^m\right)^2+\frac{h}{2|u|}\frac{\partial K(\theta^m)}{\partial\theta}\cdot\frac{\partial^2D(\theta^m)}{\partial\theta^2}\cdot\left(\sum_{ij}\frac{\partial\varphi_{pq,ij}}{\partial z}\theta_{ij}^m\right)^3\\
&\cdot\frac{h}{2|u|}\frac{\partial K(\theta^m)}{\partial\theta}\left[3\frac{\partial D(\theta^m)}{\partial\theta}\left(\sum_{ij}\frac{\partial\varphi_{pq,ij}}{\partial x}\theta_{ij}^m\right)\left(\sum_{ij}\frac{\partial^2\varphi_{pq,ij}}{\partial x^2}\theta_{ij}^m\right)+\frac{\partial^2D(\theta^m)}{\partial\theta^2}\left(\sum_{ij}\frac{\partial\varphi_{pq,ij}}{\partial x}\theta_{ij}^m\right)^3\right.\\
&+\frac{\partial D(\theta^m)}{\partial\theta}\left(\sum_{ij}\frac{\partial\varphi_{pq,ij}}{\partial x}\theta_{ij}^m\right)\left(\sum_{ij}\frac{\partial^2\varphi_{pq,ij}}{\partial z^2}\theta_{ij}^m\right)+\frac{\partial^2D(\theta^m)}{\partial\theta^2}\left(\sum_{ij}\frac{\partial\varphi_{pq,ij}}{\partial x}\theta_{ij}^m\right)\left(\sum_{ij}\frac{\partial\varphi_{pq,ij}}{\partial z}\theta_{ij}^m\right)^2\\
&+\frac{\partial D(\theta^m)}{\partial\theta}\left(\sum_{ij}\frac{\partial\varphi_{pq,ij}}{\partial z}\theta_{ij}^m\right)\left(\sum_{ij}\frac{\partial^2\varphi_{pq,ij}}{\partial x^2}\theta_{ij}^m\right)+3\frac{\partial D(\theta^m)}{\partial\theta}\left(\sum_{ij}\frac{\partial\varphi_{pq,ij}}{\partial z}\theta_{ij}^m\right)\left(\sum_{ij}\frac{\partial^2\varphi_{pq,ij}}{\partial z^2}\theta_{ij}^m\right)\\
&+\frac{\partial^2D(\theta^m)}{\partial\theta^2}\left(\sum_{ij}\frac{\partial\varphi_{pq,ij}}{\partial z}\theta_{ij}^m\right)\left(\sum_{ij}\frac{\partial\varphi_{pq,ij}}{\partial x}\theta_{ij}^m\right)^2+2\frac{\partial D(\theta^m)}{\partial\theta}\left(\sum_{ij}\frac{\partial\varphi_{pq,ij}}{\partial x}\theta_{ij}^m\right)\left(\sum_{ij}\frac{\partial^2\varphi_{pq,ij}}{\partial x\,\partial z}\theta_{ij}^m\right)\\
&\left.+2\frac{\partial D(\theta^m)}{\partial\theta}\left(\sum_{ij}\frac{\partial\varphi_{pq,ij}}{\partial z}\theta_{ij}^m\right)\left(\sum_{ij}\frac{\partial\varphi_{pq,ij}}{\partial z\,\partial x}\theta_{ij}^m\right)+\frac{\partial^2K(\theta^m)}{\partial\theta^2}\left(\sum_{ij}\frac{\partial\varphi_{pq,ij}}{\partial Z}\theta_{ij}^m\right)^2\right]+f^m+\frac{h}{2|u|}\\
&\left.\cdot\frac{\partial D(\theta^m)}{\partial\theta}\left(\frac{\partial f^m}{\partial x}+\frac{\partial f^m}{\partial z}\right)\right\}_{x=x_p,z=z_q}.
\end{aligned}
\tag{45}
$$

4. Stability

In order to analyze the stability of one-dimensional and two-dimensional time fractional soil-water movement equations, we firstly define the functional spaces endowed with standard norms and inner products:

$$
\begin{aligned}
H^1(\Omega)&=\left\{v\in L^2(\Omega),\nabla v\in L^2(\Omega)\right\},\\
H_0^1(\Omega)&=\left\{v\in H^1(\Omega),v|_{\partial\Omega}=0\right\},
\end{aligned}
\tag{46}
$$

where $L^2(\Omega)$ is the space of measurable functions whose square is Lebesgue integrable in Ω and the inner product form of $L^2(\Omega)$ is

$$
\begin{aligned}
(u,v)&=\int_\Omega u(x)v(x)dx, \qquad u,v\in L^2(\Omega),\\
(u,v)&=\int\int_\Omega u(\mathbf{x})v(\mathbf{x})dx\,dy, \quad u,v\in L^2(\Omega),
\end{aligned}
\tag{47}
$$

and the norm in $L^2(\Omega)$ is

$$\|\theta\| = (\theta,\theta)^{1/2} = \left(\int_\Omega \theta^2 dx\right)^{1/2},$$
$$\|\theta\| = (\theta,\theta)^{1/2} = \left(\int\int_\Omega \theta^2 dx\,dy\right)^{1/2}. \tag{48}$$

Lemma 1 (see [22]). *Let $\alpha \in (0,1)$, $a_l^{(\alpha)} = (l+1)^{1-\alpha} - l^{1-\alpha}$, $l = 0,1,2,\ldots$, then*

(1) $1 = a_0^{(\alpha)} > a_1^{(\alpha)} > a_2^{(\alpha)} > \cdots > a_l^{(\alpha)} > 0$; $a_l^{(\alpha)} \longrightarrow 0$, *when $l \longrightarrow \infty$;*

(2) $(1-\alpha)l^{-\alpha} < a_{l-1}^{(\alpha)} < (1-\alpha)(l-1)^{-\alpha}$, $l \geq 1$.

Lemma 1 gives the magnitude relationship of the coefficients in the time-discrete format.

Lemma 2 (see [23]). *Let $\{T_h\}$, $0 < h \leq 1$, denote a quasiuniform family of subdivisions of a polyhedral domain $\Omega \subset R^{d'}$. Let $(\widehat{K}, P, N)$ be a reference finite element space such that $P \subset W^{l,p}(\widehat{K}) \cap W^{m,q}(\widehat{K})$ is a finite-dimensional space of functions on $\widehat{K}$, N is a basis for P', where $1 \leq p \leq \infty$, $1 \leq q \leq \infty$, and $0 \leq m \leq l$. For $K \in T_h$, let (K, P_K, N_K) be the affine equivalent element, and $V_h = \{v$: v is measurable and $v \mid K \in P_K$, $\forall K \in T_h\}$. Then, there exists $C = C(l,p,q)$ such that*

$$\left[\sum_{K\in T_h} \|v\|^p_{W^{i,p}(K)}\right]^{1/p} \leq Ch^{m-l+\min\left(0,\left(d'/p\right)-\left(d'/q\right)\right)}\left[\sum_{K\in T_h} \|v\|^q_{W^{m,q}(K)}\right]^{1/q}. \tag{49}$$

for all $v \in V_h$.

Lemma 3 (see [24]). *Let Ω be a given region with boundary $\partial\Omega$, T_h be a uniform partition on Ω, h is the size of unit e in T_h, and the finite element space $V_h = \{v : v \mid e \in P_k(e), \forall e \in T_h$ on T_h, where P_k is a polynomial space whose number of times does not exceed k; then, for the function $u_h \in V_h$ in the finite element space, there exists a constant C independent of h satisfying*

$$\|u_h\|_{k,p,\Omega} \leq Ch^{l-k+n((1/p)-(1/q))}\|u_h\|_{l,q,\Omega}, \tag{50}$$

where $l \leq k$, $q \leq p$, and n is the dimension.

Lemmas 2 and 3 refer to the inverse inequality of finite element, but their forms are different. In the discussion of stability, we use the classical finite element inverse estimation inequality; that is, let Ω be a given region with boundary $\partial\Omega$, T_h be a uniform partition on Ω, h is the size of unit e in T_h, and the finite element space $V_h = \{v : v \mid e \in P_k(e), \forall e \in T_h$ on T_h, where P_k is a polynomial space whose number of times does not exceed k; then for the function $u_h \in V_h$ in the finite element space, there exists a constant C independent of h satisfying:

$$\|\nabla u_h\| \leq Ch^{-1}\|u_h\|. \tag{51}$$

Lemma 4 (see [25]). *If V_h is a two-dimensional linear finite element space, then when $C_0 = \sqrt{12}$ ($C_0 = 12$), there is*

$$\|\nabla u_h\|_{0,2} \leq C_0 h^{-1}\|u_h\|_{0,2}, \tag{52}$$

where $m = 0$, $p = 2$ in $\|u\|_{m,p,\Omega}$, and for any $C < C_0$, there is $u_h \in V_h$ such that [52] does not hold.

Based on Lemmas 2 and 3, a special case of the finite element inverse estimation inequality is given Lemma 4; that is, when V_h is a linear finite element space, the constant C_0 in the inverse estimation inequality is a specific number.

Lemma 5 (see [26]). *Given $E(t) \leq \rho(t) + C\int_0^T E(s)ds$, thanks to the integral form of Gronwall's inequality, it is derived that*

$$E(t) \leq \rho(t)e^{CT}, \quad 0 < t \leq T. \tag{53}$$

4.1. In the One-Dimensional Case. The time-discrete scheme of equation (1) is shown in equation (30). When discussing the stability of equation (30), we used the finite element inverse estimation inequality, and the finite element inverse estimation inequality was discussed in the finite element space (see Lemmas 2 and 3). Therefore, we choose the finite element space. From Lemmas 2 and 3, the finite element space can be defined as $V_h \subset H_0^1$, where

$$V_h = \left\{v \in H_0^1(\Omega) \cap C^0(\overline{\Omega}) \mid v\mid_e \in P_k(e), \forall e \in T_h\right\}. \tag{54}$$

Theorem 1. *Suppose $\theta^m \in V_h \subset H_0^1(\Omega)$, $m = 0,1,2,\ldots,n$. θ^m is the numerical solution of equation (1); then*

$$\|\theta^m\| \leq C\|\theta^0\| + \lambda C \max_{0\leq l\leq n}\|f^l\|, \tag{55}$$

where C is a positive constant.

Proof. We will prove the above result by mathematical induction.

For $m = 1$, we have

$$a_0^{(\alpha)}\theta^1 - a_0^{(\alpha)}\theta^0 = \lambda\frac{\partial}{\partial z}\left(D\left(\theta^1\right)\frac{\partial\theta^1}{\partial z}\right) + \lambda\frac{\partial K\left(\theta^1\right)}{\partial z} + \lambda f^1, \tag{56}$$

where $\lambda = \tau^\alpha\Gamma(2-\alpha)$.

Multiplying equation (56) by θ^1 and integrating on Ω, and then using integration by parts, we have

$$\begin{aligned}\left(a_0^{(\alpha)}\theta^1,\theta^1\right) &= a_0\left(\theta^0,\theta^1\right) - \lambda\left(D\left(\theta^1\right),\left(\frac{\partial\theta^1}{\partial z}\right)^2\right)\\ &\quad - \lambda\left(K\left(\theta^1\right),\frac{\partial\theta^1}{\partial z}\right) + \lambda\left(f^1,\theta^1\right).\end{aligned} \tag{57}$$

Due to $0 < m \leq D(\theta) \leq M$, $|K(\theta)| \leq L|\theta|$, and $|K'(\theta)| \leq L$,

$$\|\theta^1\|^2 \leq a_0\left(\theta^0,\theta^1\right) + \lambda\left(M,\left(\frac{\partial\theta^1}{\partial z}\right)^2\right) + \lambda\left(f^1,\theta^1\right). \tag{58}$$

From Lemma 1, we have

$$\|\theta^1\|^2 \le (\theta^0, \theta^1) + \lambda\left(M, \left(\frac{\partial\theta^1}{\partial z}\right)^2\right) + \lambda(f^1, \theta^1). \tag{59}$$

Using Schwarz's inequality and the inverse inequality in Lemmas 2 and 3, we obtain

$$\begin{aligned}\|\theta^1\|^2 &\le \|\theta^0\|\|\theta^1\| + \lambda M\left\|\left(\frac{\partial\theta^1}{\partial z}\right)^2\right\| + \lambda\|f^1\|\|\theta^1\| \le \|\theta^0\|\|\theta^1\| \\ &\quad + \lambda M c h^{-2}\|\theta^1\|^2 + \lambda\|f^1\|\|\theta^1\|,\end{aligned} \tag{60}$$

hence,

$$(1 - \lambda M c h^{-2})\|\theta^1\| \le \|\theta^0\| + \lambda \max_{0\le l\le n}\|f^l\|, \tag{61}$$

when $1 - \lambda M c h^{-2} > 0$, then

$$\|\theta^1\| \le C\|\theta^0\| + \lambda C \max_{0\le l\le n}\|f^l\|. \tag{62}$$

Suppose that now we have proven

$$\|\theta^k\| \le C\|\theta^0\| + \lambda C \max_{0\le l\le N}\|f^l\|, \quad k = 1, 2, 3, \ldots, m-1. \tag{63}$$

Multiplying equation (30) by θ^m and integrating on Ω, and then using integration by parts, we have

$$\begin{aligned}(\theta^m, \theta^m) &= \sum_{k=1}^{m-1}\left(a_{m-k-1}^{(\alpha)} - a_{m-k}^{(\alpha)}\right)(\theta^k, \theta^m) + a_{m-1}^{(\alpha)}(\theta^0, \theta^m) \\ &\quad - \lambda\left(D(\theta^m), \left(\frac{\partial\theta^m}{\partial z}\right)^2\right) - \lambda\left(K(\theta^m), \left(\frac{\partial\theta^m}{\partial z}\right)^2\right) \\ &\quad + \lambda(f^m, \theta^m).\end{aligned} \tag{64}$$

By a derivation process similar to $m = 0$, we obtain

$$\begin{aligned}(1 - \lambda M c h^{-2})\|\theta^m\| &\le \sum_{k=1}^{m-1}\left(a_{m-k-1}^{(\alpha)} - a_{m-k}^{(\alpha)}\right)\|\theta^k\| + a_{m-1}^{(\alpha)}\|\theta^0\| \\ &\quad + \lambda \max_{0\le l\le n}\|f^l\| \\ &\le \sum_{k=1}^{m-1}\left(a_{m-k-1}^{(\alpha)} - a_{m-k}^{(\alpha)}\right)\left(C\|\theta^0\| + \lambda C \max_{0\le l\le n}\|f^l\|\right) \\ &\quad + a_{m-1}^{(\alpha)}\|\theta^0\| + \lambda \max_{0\le l\le n}\|f^l\| \\ &\le \left(C\left(a_0^{(\alpha)} - a_{m-1}^{(\alpha)}\right) + a_0^{(\alpha)}\right)\|\theta^0\| \\ &\quad + \lambda\left(C\left(a_0^{(\alpha)} - a_{m-1}^{(\alpha)}\right) + a_0^{(\alpha)}\right)\max_{0\le l\le n}\|f^l\| \\ &\le C\|\theta^0\| + \lambda C \max_{0\le l\le n}\|f^l\|.\end{aligned} \tag{65}$$

Due to $1 - \lambda M c h^{-2} > 0$,

$$\|\theta^m\| \le C\|\theta^0\| + \lambda C \max_{0\le l\le n}\|f^l\|, \tag{66}$$

and the proof is finished. □

4.2. In the Two-Dimensional Case. The time-discrete scheme of equation (3) is shown in equation (41). When discussing the stability of equation (41), we choose the finite element space, which is defined as equation (56).

Theorem 2. *Suppose $\theta^m \in V_h \subset H_0^1(\Omega)$, $m = 0, 1, 2, \ldots, n$. θ^m is the numerical solution of equation (3); then*

$$\|\theta^m\| \le \rho e^{CT}, \tag{67}$$

where C and ρ are positive constants.

Proof. Multiplying equation (41) by θ^m and integrating on Ω, and then using Green's formula, we have

$$\begin{aligned}(\theta^m, \theta^m) &= \sum_{k=1}^{m-1}\left(a_{m-k-1}^{(\alpha)} - a_{m-k}^{(\alpha)}\right)(\theta^k, \theta^m) + a_n^{(\alpha)}(\theta^0, \theta^m) \\ &\quad - \lambda\left(D(\theta^m)\frac{\partial\theta^m}{\partial x}, \frac{\partial\theta^m}{\partial x}\right) - \lambda\left(D(\theta^m)\frac{\partial\theta^m}{\partial z}, \frac{\partial\theta^m}{\partial z}\right) \\ &\quad + \lambda\left(\frac{\partial K(\theta^m)}{\partial z}, \theta^m\right) + \lambda(f^m, \theta^m).\end{aligned} \tag{68}$$

By $0 < m \le D(\theta) \le M$, $|K(\theta)| \le L|\theta|$, $|K'(\theta)| \le L$, and Schwarz inequality, we obtain

$$\begin{aligned}\|\theta^m\|^2 + 2\lambda M\left\|\frac{\partial\theta^m}{\partial x}\right\|\left\|\frac{\partial\theta^m}{\partial z}\right\| &\le \sum_{k=1}^{m-1}\left(a_{m-k-1}^{(\alpha)} - a_{m-k}^{(\alpha)}\right)\|\theta^k\|\|\theta^m\| \\ &\quad + a_{m-1}^{(\alpha)}\|\theta^0\|\|\theta^m\| + \lambda M\left\|\frac{\partial\theta^m}{\partial x}\right\|^2 \\ &\quad + \lambda M\left\|\frac{\partial\theta^m}{\partial z}\right\|^2 + 2\lambda M\left\|\frac{\partial\theta^m}{\partial x}\right\|\left\|\frac{\partial\theta^m}{\partial z}\right\| \\ &\quad + \lambda L\left\|\frac{\partial\theta^m}{\partial z}\right\|\|\theta^m\| + \lambda\|f^m\|\|\theta^m\|.\end{aligned} \tag{69}$$

For the derivative part on the right side of the inequality, using the inverse inequality in Lemmas 2 and 3, there is

$$\begin{aligned}\lambda M\left\|\frac{\partial\theta^m}{\partial x}\right\|^2 + 2\lambda M\left\|\frac{\partial\theta^m}{\partial x}\right\|\left\|\frac{\partial\theta^m}{\partial z}\right\| + \lambda M\left\|\frac{\partial\theta^m}{\partial z}\right\|^2 + \lambda L\left\|\frac{\partial\theta^m}{\partial z}\right\|\|\theta^m\| \\ \le \lambda M c_1 h^{-2}\|\theta^m\|^2 + \lambda L c_2 h^{-1}\|\theta^m\|^2.\end{aligned} \tag{70}$$

Hence,

$$\begin{aligned}(1 - \lambda M c_1 h^{-2} - \lambda L c_2 h^{-1})\|\theta^m\| &\le \sum_{k=1}^{m-1}\left(a_{m-k-1}^{(\alpha)} - a_{m-k}^{(\alpha)}\right)\|\theta^k\| \\ &\quad + a_{m-1}^{(\alpha)}\|\theta^0\| + \lambda\|f^m\|,\end{aligned} \tag{71}$$

when $1 - \lambda M c_1 h^{-2} - \lambda L c_2 h^{-1} \ge 0$, we have

$$\begin{aligned}\|\theta^m\| \le{}& \frac{1}{1-\lambda M c_1 h^{-2}-\lambda L c_2 h^{-1}} \sum_{k=1}^{m-1}\left(a_{m-k-1}^{(\alpha)}-a_{m-k}^{(\alpha)}\right)\|\theta^k\| \\ &+\frac{a_{m-1}^{(\alpha)}}{1-\lambda M c_1 h^{-2}-\lambda L c_2 h^{-1}}\|\theta^0\| \\ &+\frac{\lambda}{1-\lambda M c_1 h^{-2}-\lambda L c_2 h^{-1}}\|f^m\|.\end{aligned} \tag{72}$$

Assume $C_2 = \max_{1\le k\le m-1}\{|a_{m-k-1}^{(\alpha)} - a_{m-k}^{(\alpha)}|\}$, there is

$$\begin{aligned}\|\theta^m\| \le{}& \frac{C_2}{1-\lambda M c_1 h^{-2}-\lambda L c_2 h^{-1}} \sum_{k=1}^{m-1}\|\theta^k\| \\ &+\frac{1}{1-\lambda M c_1 h^{-2}-\lambda L c_2 h^{-1}}\left(a_{m-1}^{(\alpha)}\|\theta^0\|+\lambda\|f^m\|\right) \\ ={}& C\sum_{k=1}^{m-1}\|\theta^k\| + D\left(a_{m-1}^{(\alpha)}\|\theta^0\|+\lambda\|f^m\|\right) = C\sum_{k=1}^{m-1}\|\theta^k\| + \rho.\end{aligned} \tag{73}$$

i.e.,

$$\|\theta^m\| \le \rho + C\sum_{k=1}^{m-1}\|\theta^k\|. \tag{74}$$

Applying Lemma 5, we obtain

$$\|\theta^m\| \le \rho e^{CT}. \tag{75}$$

□

5. Results and Discussion

In this section, we show the results for two examples using the method described in previous sections. To show the accuracy of the proposed method, maximum absolute error and relative error are presented as

$$\begin{aligned}\varepsilon_1 &= \max_{1\le i\le N}\left|\theta(\mathbf{z}_i) - \theta_{\text{exact}}(\mathbf{z}_i)\right|, \\ \varepsilon_2 &= \sqrt{\frac{\sum_{i=1}^{N}\left[\theta(\mathbf{z}_i)-\theta_{\text{exact}}(\mathbf{z}_i)\right]^2}{\sum_{i=1}^{N}\left[\theta(\mathbf{z}_i)\right]^2}},\end{aligned} \tag{76}$$

where $\theta(\mathbf{z}_i)$ and $\theta_{\text{exact}}(\mathbf{z}_i)$ for $i = 1, 2, \ldots, N$ are computed by the exact and numerical solutions on points $\mathbf{z}_i$, respectively, and N is the number of nodal points.

Gaussian function has arbitrary order derivative. We choose Gaussian function as the weight function, and the basis function is quadratic basis function $\mathbf{p}^{\mathrm{T}} = (1, \mathbf{x}, \mathbf{x}^2)$ in the example.

Example 1. Consider one-dimensional time fractional soil water movement equation

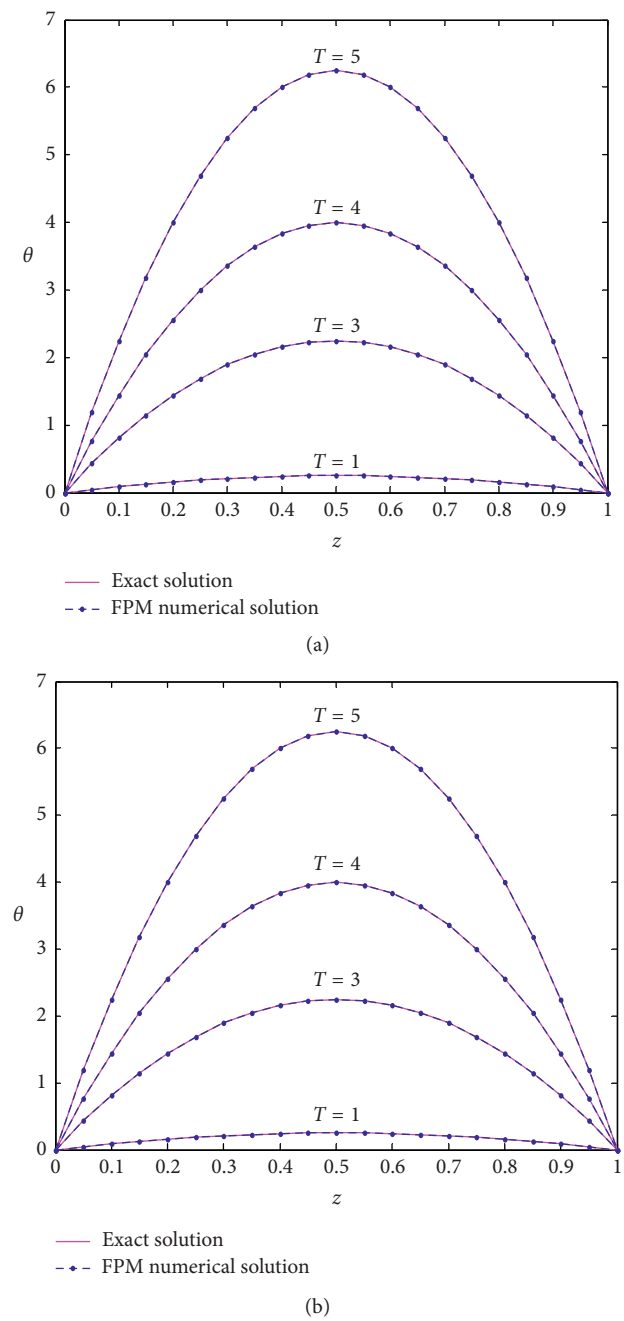

Figure 1: Comparing the proposed method with the exact solution when $\Delta t = 10^{-3}$ and the number of nodes is 21, where $\alpha = 0.5$ (a), $\alpha = 0.8$ (b).

$$\begin{cases} {}_0^C D_t^\alpha \theta = \dfrac{\partial}{\partial z}\left(D(\theta)\dfrac{\partial\theta}{\partial z}\right) + \dfrac{\partial K(\theta)}{\partial z} + f, & (z,t) \in [0,1]\times[0,T], \\ \theta(z,0) = 0, & z \in [0,1], \\ \theta(0,t) = 0, & t \in [0,T), \\ \theta(1,t) = 0, & t \in (0,T], \end{cases} \tag{77}$$

where $K(\theta) = \theta, D(\theta) = 0.001\theta + 0.001$, the exact solution is $\theta = t^2(z - z^2)$, and $f(x)$ can be obtained by substituting the exact solution into the equation.

We take $\Delta t = 10^{-3}$, the basis function is quadratic basis function $p^T = (1, x, x^2)$ and scale is 2.5 in Example 1.

Figure 1 shows the comparison between the FPM and the exact solution at different times when $\alpha = 0.5$ and $\alpha = 0.8$, respectively. It can be seen from Figure 1 that the finite point numerical solution and the exact solution can still agree well even when T is large.

Table 1 shows the $\varepsilon 2$ errors of the FPM and the FDM under different α when $T = 1$, $\Delta t = 10^{-3}$, and the number of nodes is 11. It can be seen from Table 1 that as α increases, the $\varepsilon 2$ errors of both the FPM and the FDM increase gradually, but the $\varepsilon 2$ errors of the FPM is significantly smaller than the FDM.

When $\alpha = 0.8$, Table 2 gives the $\varepsilon 2$ errors of the FPM and the FDM under different node numbers at $T = 1$. Table 3 gives the $\varepsilon 2$ errors of the FPM and the FDM at different times. Table 4 verifies the convergence order of the FPM. As can be seen from Table 2, with the increase of the number of spatial nodes, the numerical solution is closer to the exact solution, and the $\varepsilon 2$ errors of the FPM are still higher than those of the FDM. It can be seen from Table 3 that the $\varepsilon 2$ errors of the FPM and the FDM decrease gradually with the increase of time, but the results of proposed method are still better than those of the FDM and the $\varepsilon 2$ errors can still reach the order of $e - 005$ when $T = 2$, which shows that the proposed method can obtain relatively stable results in simulating water infiltration process. From Table 4, it can be seen that the convergence order is closer to 1.2 as the time step decreases when $\alpha = 0.8$, which shows that the convergence order is closer to the theoretical convergence order.

Example 2. Consider one-dimensional time fractional soil water movement equation:

$$\begin{cases} {}_0^C D_t^\alpha \theta = \dfrac{\partial}{\partial x}\left(D(\theta)\dfrac{\partial \theta}{\partial x}\right) + \dfrac{\partial}{\partial z}\left(D(\theta)\dfrac{\partial \theta}{\partial z}\right) + \dfrac{\partial K(\theta)}{\partial z} + f, & (x, z, t) \in [0,1] \times [0,1] \times [0, T], \\ \theta(x, z, 0) = (x - x^2)(z - z^2), & (x, z) \in [0,1] \times [0, L], \\ \theta(0, z, t) = 0, & (z, t) \in [0,1] \times [0, T], \\ \theta(1, z, t) = 0, & (z, t) \in [0,1] \times [0, T], \\ \theta(x, 0, t) = 0, & (z, t) \in [0,1] \times [0, T], \\ \theta(x, 1, t) = 0, & (z, t) \in [0,1] \times [0, T], \end{cases} \tag{78}$$

where $K(\theta) = \theta, D(\theta) = 0.001\theta + 0.001$, the exact solution is $\theta = t^2(x - x^2)(z - z^2)$, and $f(x)$ can be obtained by substituting the exact solution into the equation.

We take Δt is 10^{-3}, the basis function is quadratic basis function $\mathbf{p}^{\mathrm{T}} = (1, \mathbf{x}, \mathbf{x}^2)$, and scale is 2 in Example 2.

When $T = 1$ and $\alpha = 0.8$, Figure 2 gives the comparison between the numerical solution of FPM and the exact solution when the number of nodes is 21×21. Figure 3 gives the equipotentia of the exact solution and the numerical solution when the number of nodes is 31×31. From Figure 3, we can see that the numerical solution of FPM is basically consistent with the exact solution.

Table 5 shows the $\varepsilon 2$ errors of the FPM and the FDM under different α when $T = 1$, $\Delta t = 10^{-3}$, and the number of nodes is 21×21. It can be seen from Table 5 that as α increases, the $\varepsilon 2$ errors of the FPM is significantly smaller than the FDM. when $\alpha = 0.8$. Table 6 gives the $\varepsilon 2$ errors of the FPM and the FDM under different number of nodes. From Table 6, we can see that the $\varepsilon 2$ errors of proposed method and the FDM can reach the same order of magnitude when the number of nodes is small, but with the increase of the number of nodes, the errors of the FPM decreases faster than those of the FDM. Table 7 gives the $\varepsilon 2$ errors of the FPM and the FDM at different times. It can be seen from Table 7 that when $T = 2$, the results of the FPM are still better than those of the FDM, and the $\varepsilon 2$ errors can still reach the order of magnitude of $e - 004$. Table 8 verifies the convergence order of the FPM. From Table 8, it can be seen that the convergence order is closer to 1.2 as the time step decreases when $\alpha = 0.8$.

Table 1: Comparison of $\varepsilon 2$ errors between the FPM and the FDM under different α, when $T=1$, $\Delta t=10^{-3}$, and the number of nodes is 11.

α	0.4	0.5	0.6	0.7	0.8
FPM	$2.5156e-06$	$6.9681e-06$	$1.8722e-05$	$4.7683e-05$	$1.1539e-04$
FDM	$1.4281e-03$	$1.4360e-03$	$1.4519e-03$	$1.4823e-03$	$1.5359e-03$

Table 2: Comparison of $\varepsilon 2$ errors between FPM and FDM under different node numbers, when $\alpha=0.8$.

Time step	Time	Number of nodes	FPM	FDM
0.001	1	11	$1.1539e-04$	$1.5339e-03$
		21	$1.0193e-04$	$1.4928e-03$
		41	$9.6788e-05$	$1.4326e-03$
		81	$9.5715e-05$	$1.4027e-03$

Table 3: Comparison of $\varepsilon 2$ errors between FPM and FDM under different times, when $\alpha=0.8$.

Time step	Number of nodes	Time	FPM	FDM
0.001	21	0.1	$3.1502e-03$	$5.5855e-03$
		0.5	$3.4321e-04$	$2.5670e-03$
		1.0	$1.0193e-04$	$1.4928e-03$
		2.0	$2.7596e-05$	$8.0918e-04$

Table 4: $\varepsilon 1$ errors and convergence order of numerical solution, when $\alpha=0.8$ and the number of nodes is 11.

Time step	$\varepsilon 1$	Convergence rate
1/20	$3.3612e-03$	
1/40	$1.5831e-03$	1.0862
1/80	$7.4187e-04$	1.0935
1/160	$3.4394e-04$	1.1090
1/320	$1.5711e-04$	1.1304
1/640	$7.0722e-05$	1.1515

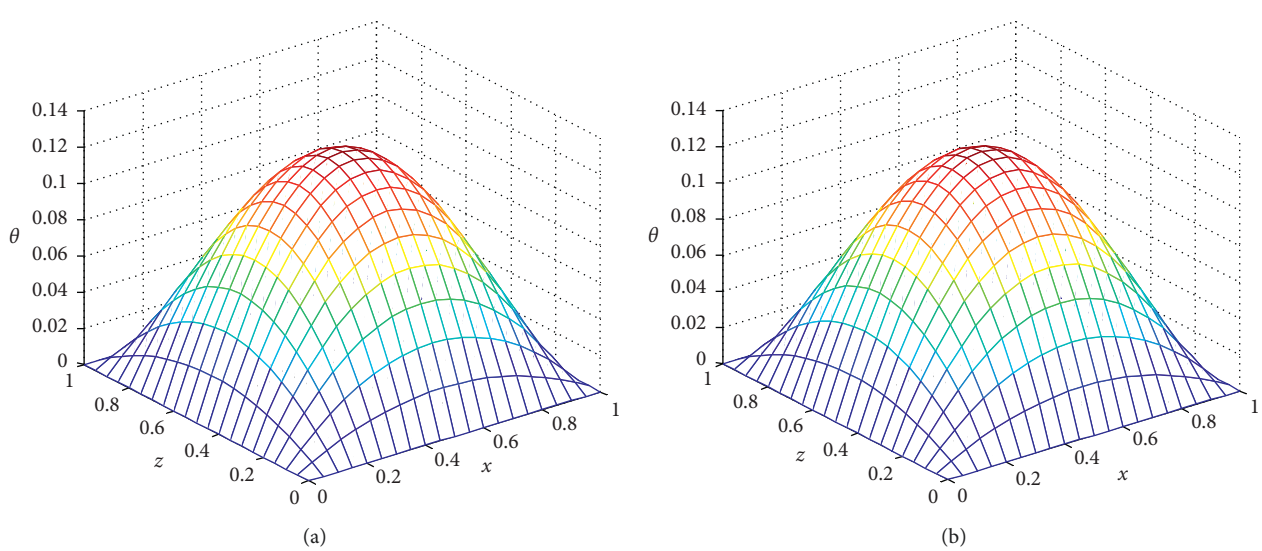

Figure 2: Comparing the proposed method with the exact solution when $T=1$, $\Delta t=10^{-3}$, $\alpha=0.8$, and the number of nodes is 21×21. (a) Exact solution. (b) FPM numerical solution.

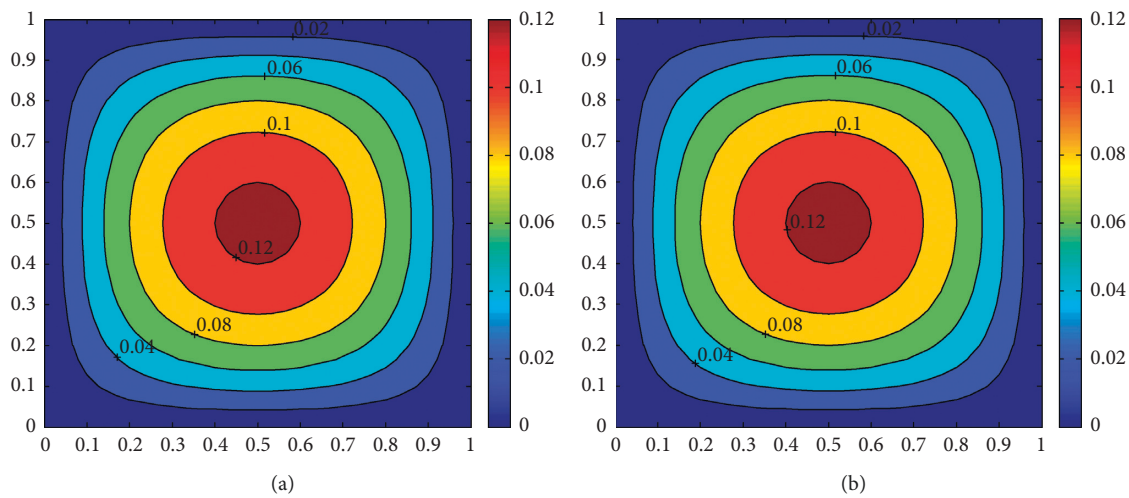

Figure 3: The equipotentia of the exact solution and the numerical solution of FPM when $T = 1$, $\Delta t = 10^{-3}$, $\alpha = 0.8$, and the number of nodes is 31×31. (a) FPM numerical solution. (b) Exact numerical.

Table 5: Comparison of $\varepsilon 2$ errors between the FPM and the FDM under different α, when $T = 1$, $\Delta t = 10^{-3}$, and the number of nodes is 21×21.

α	0.4	0.5	0.6	0.7	0.8
FPM	$1.4446e-04$	$1.4556e-04$	$1.4688e-04$	$1.4846e-04$	$1.5078e-04$
FDM	$7.7600e+03$	$3.9952e-04$	$4.0953e-04$	$4.2217e-04$	$4.4397e-04$

Table 6: Comparison of $\varepsilon 2$ errors between FPM and FDM under different node numbers, when $\alpha = 0.8$.

Time step	Time	Number of nodes	FPM	FDM
0.001	1	11×11	$8.5446e-04$	$4.4956e-04$
		21×21	$1.5078e-04$	$4.4397e-04$
		31×31	$5.1900e-05$	$4.4465e-04$
		41×41	$2.3658e-05$	$4.4233e-04$

Table 7: Comparison of $\varepsilon 2$ errors between FPM and FDM under different times, when $\alpha = 0.8$.

Time step	Number of nodes	Time	FPM	FDM
0.001	21×21	0.01	$1.5661e-05$	$6.9692e-05$
		0.1	$7.5940e-05$	$4.0981e-04$
		1.0	$1.5078e-04$	$4.4397e-04$
		2.0	$1.6702e-04$	$2.9891e-04$

Table 8: $\varepsilon 1$ errors and convergence order of numerical solution, when $\alpha = 0.8$ and the number of nodes is 21×21.

Time step	$\varepsilon 1$	Covergence rate
1/10	$1.8574e-04$	
1/20	$1.0418e-04$	0.8342
1/40	$5.7024e-05$	0.8694
1/80	$2.7958e-05$	1.0283
1/160	$1.3560e-05$	1.0440

6. Conclusions

In this article, the finite point method (FPM) was applied to the time fractional Richards' equation in one- and two-dimensional cases. We have discretized the time fractional derivative using a finite difference formula and obtained a time-discrete scheme which proved to be conditionally stable. One- and two-dimensional numerical examples were given. Compared with finite difference method, the accuracy of finite point method was better than that of finite difference method. Meanwhile, numerical examples showed that the proposed method is simple and effective.

Data Availability

No data were used to support this study.

Conflicts of Interest

The authors declare that there are no conflicts of interest regarding the publication of this paper.

Acknowledgments

This research was supported by the National Natural Research Foundation of China (51979220).

References

[1] Y. Pachepsky, D. Timlin, and W. Rawls, "Generalized Richards' equation to simulate water transport in unsaturated soils," *Journal of Hydrology*, vol. 272, no. 1–4, pp. 3–13, 2003.

[2] E. Gerolymatou, I. Vardoulakis, and R. Hilfer, "Modelling infiltration by means of a nonlinear fractional diffusion model," *Journal of Physics D Applied Physics*, vol. 39, no. 18, pp. 4104–4110, 2006.

[3] X. Qin, X. Duan, L. Su, X. Shen, and G. Hu, "Numerical simulation of soil water movement under subsurface irrigation," *Mathematical Problems in Engineering*, vol. 2014, Article ID 126398, p. 9, 2014.

[4] J. Wang, L. Su, and X. Qin, "Hermite radial basis collocation method for unsaturated soil water movement equation," *Mathematical Problems in Engineering*, vol. 2018, Article ID 8298915, p. 19, 2018.

[5] X. Qin, X. Duan, G. Hu, L. Su, and X. Wang, "An Element-free Galerkin method for solving the two-dimensional hyperbolic problem," *Applied Mathematics and Computation*, vol. 312, pp. 106–120, 2018.

[6] W. Chen, L. Ye, and H. Sun, "Fractional diffusion equations by the Kansa method," *Computers & Mathematics with Applications*, vol. 59, no. 5, pp. 1614–1620, 2010.

[7] A. A. Freitas, D. G. A. Vigo, M. G. Teixeira, and C. A. B. d. Vasconcellos, "Horizontal water flow in unsaturated porous media using a fractional integral method with an adaptive time step," *Applied Mathematical Modelling*, vol. 48, pp. 584–592, 2017.

[8] M. Dehghan, M. Abbaszadeh, and A. Mohebbi, "An implicit RBF meshless approach for solving the time fractional nonlinear Sine-Gordon and Klein-Gordon equations," *Engineering Analysis with Boundary Elements*, vol. 50, pp. 412–434, 2015.

[9] A. Tayebi, Y. Shekari, and M. H. Heydari, "A meshless method for solving two-dimensional variable-order time fractional advection-diffusion equation," *Journal of Computational Physics*, vol. 340, pp. 655–669, 2017.

[10] A. Mardani, M. R. Hooshmandasl, M. H. Heydari, and C. Cattani, "A meshless method for solving the time fractional advection-diffusion equation with variable coefficients," *Computers & Mathematics with Applications*, vol. 75, no. 1, pp. 122–133, 2018.

[11] T. Liu, G. Liu, and J. Zhu, "Advances in the studies on Meshless methods," *Chinese Journal of Mechanical Engineering*, vol. 38, no. 5, pp. 7–12, 2002, in Chinese with English abstract.

[12] E. Oñate, S. Idelsohn, O. C. Zienkiewicz, R. L. Taylor, and C. Sacco, "A stabilized finite point method for analysis of fluid mechanics problems," *Computer Methods in Applied Mechanics and Engineering*, vol. 139, no. 1–4, pp. 315–346, 1996.

[13] E. Oñate, S. Idelsohn, O. C. Zienkiewicz et al., "A finite point method in computational mechanics applications to convective transport and fluid flow," *International Journal for Numerical Methods in Engineering*, vol. 39, no. 22, pp. 3839–3866, 2015.

[14] S. Tiwari and J. Kuhnert, "Finite pointset method based on the projection method for simulations of the incompressible Navier-Stokes equations," *Lecture Notes in Computational Science and Engineering*, vol. 26, pp. 373–387, 2003.

[15] A. Shojaei, F. Mossaiby, M. Zaccariotto, and U. Galvanetto, "The meshless finite point method for transient elastodynamic problems," *Acta Mechanica*, vol. 228, no. 10, pp. 3581–3593, 2017.

[16] M. Kamranian, M. Dehghan, and M. Tatari, "Study of the two-dimensional Sine-Gordon equation arising in Josephson junctions using meshless finite point method," *International Journal of Numerical Modelling Electronic Networks Devices and Fields*, vol. 30, no. 6, p. 2210, 2017.

[17] J. Li and X. Qin, "Finite point method for the time fractional convection-diffusion equation," *Advances in Intelligent Systems and Computing*, vol. 877, pp. 28–36, 2019.

[18] M. A. Noor and M. Waseem, "Some iterative methods for solving a system of nonlinear equations," *Computers and Mathematics with Applications*, vol. 57, no. 1, pp. 101–106, 2009.

[19] I. Boglaev, "Monotone iterative ADI method for solving coupled systems of nonlinear parabolic equations," *Applied Numerical Mathematics*, vol. 108, pp. 204–222, 2016.

[20] A. Amiri, A. Cordero, M. T. Darvishi, and J. R. Torregrosa, "A fast algorithm to solve systems of nonlinear equations," *Journal of Computational and Applied Mathematics*, vol. 354, pp. 242–258, 2019.

[21] A. Bahl, A. Cordero, R. Sharma, and J. R. Torregrosa, "A novel bi-parametric sixth order iterative scheme for solving nonlinear systems and its dynamics," *Applied Mathematics and Computation*, vol. 357, pp. 147–166, 2019.

[22] Z. Sun and G. Gao, *Finite Difference Method for Fractional Differential Equations*, Science Press, Beijing, China, 2015.

[23] S. C. Brenner and L. R. Scott, *The Mathematical Theory of Element Methods*, Springer-Verlag, Berlin, Germany, 1994.

[24] Q. Lin and N. Yan, *Construction and Analysis of High Efficiency Finite Element Method*, Hebei University Press, Baoding, China, 1996.

[25] J. Tan and W. He, "Bound of constant factor in the estimated inverse inequality the finite element space," *Journal of Wenzhou University Naturnal Sciences*, vol. 30, no. 3, pp. 7–13, 2009, in Chinese with English abstract.

[26] R. Zheng, X. Jiang, and H. Zhang, "L1 Fourier spectral methods for a class of generalized two-dimensional time fractional nonlinear anomalous diffusion equations," *Computers & Mathematics with Applications*, vol. 75, no. 5, pp. 1515–1530, 2018.